Check for updates

Original Article

Institution of MECHANICAL ENGINEERS
Journal of MECHANICAL ENGINEERING SCIENCE

Proc IMechE Part C:
J Mechanical Engineering Science
2021, Vol. 235(2) 381–390
© IMechE 2020
Article reuse guidelines:
sagepub.com/journals-permissions
DOI: 10.1177/0954406220946062
journals.sagepub.com/home/pic
SAGE

An IB-LBM design of a microfluidics-based cell capture system

Jing-Tao Ma[1,2,*], Wen-Hong Zu[3,*], Xiao-Ying Tang[1] and Yuan-Qing Xu[1]

Abstract

The capture of cells in a microfluidic device based on U-shaped sieves is numerically investigated by the immersed boundary-lattice Boltzmann method (IB-LBM). The effects of the width of the inlet (h), the radius of sieves (r_2), and the radius of posts (r_1) on the efficiency of the device on trapping cells are studied. It is found that a narrower inlet improves the capability of the device to capture cells and promotes the uniform trapping of cells. In addition, the device is not sufficiently efficient in capturing cells when the radius r_2 is small. By increasing r_2 gradually, the cells trapped in the device are found to grow up first and then decrease. This can be explained as an optimal size of apertures between posts to induce the cells to enter the sieve, and then the cells can plug up these apertures. Finally, the effects of the post size on the cell-capturing are studied. It is found that more cells can be captured as r_1 experiences a slight increase, while the capturing efficiency will not improve if continuing to increase r_1.

Keywords

Cell capture, microfluidic chip, Lattice Boltzmann method, immersed boundary method

Date received: 19 April 2020; accepted: 7 July 2020

Introduction

Microfluidics has many advantages over conventionally sized techniques for its low cost, low sample requirement, high integration and high efficiency. Cell manipulation (e.g. cell capture, separation, and focusing) based on microfluidics has enjoyed great popularity in recent decades, among which cell capture is a necessary step for many subsequent applications such as cell counting, cell culture, and disease diagnosis.

In order to achieve the efficient capture of cells, different designs have been proposed including active techniques (which normally require external fields, such as optical,[1] acoustic[2,3] and electric[4,5] fields) and passive techniques[6–9] (which simply rely on the structure of the microfluidic device and hydrodynamic forces). Compared to passive techniques, active techniques commonly involve higher costs as they require additional devices to produce external fields, and some additional work may be needed in active techniques such as the magnetic labeling of non-magnetic particles.[10] On the contrary, passive techniques are simpler and easy to implement. So they have attracted more attention in the past years, such as the inertial focusing of microparticles,[11] the separation of blood cells via the pinched flow,[12] or the crossflow.[13] However, these applications mainly deal with moving particles. In order to trap floating cells from the flow, some specially designed architectures are usually required. For example, Kim and his collaborators proposed a U-shaped sieve-based technique to trap and culture the BALB/3T3 cell.[8,9] They developed a Lagrangian method to simulate the motion of cells in the microfluidic device, and their simulation results showed qualitative agreement with experiments. Their studies also indicate that the flow rules are significant to help the practical design. However, in the modeling of cell manipulation in microscale, it is better to consider the effects of cells on the fluid flow, as reported in previous studies.[14,15] This is because a cell can significantly influence the fluid flow in microscale. Therefore, it would be

[1]School of Life Science, Beijing Institute of Technology, Beijing, China
[2]School of Engineering and Information Technology, University of New South Wales, Canberra, Australia
[3]Institute of Hepatology, National Clinical Research Center for Infectious Disease, Shenzhen Third People's Hospital, Shenzhen, China

*These two authors contributed equally to this work.

Corresponding author:
Yuan-Qing Xu, School of Life Science, Beijing Institute of Technology 5 South Zhongguancun Street, Haidian District, Beijing 100081, China.
Email: bitxyq@bit.edu.cn

desirable to include the effects of cells on fluid behaviors in the investigation of cell capture in a microfluidic device.

Over the last several decades, many efforts have been made on experimental and numerical investigations on cell behaviors in fluids. The experimental studies on the dynamics of cells can be dated back to the 1960s, when red blood cells were found to experience tank-treading movements in a shear flow.[16] Later, it was found that a cell may also undergo swinging[17] and tumbling[18] motions. In contrast, numerical investigations on cell behaviors were much later (from the 1990s). Early attempts to numerically study cell behaviors normally involve the boundary element method (BEM). Specifically, Pozrikidis and his coworkers have numerically investigated behaviors of 2D and 3D capsules in different flow conditions (e.g. shear flows[19,20] and extensional flows[21]). Barthes-Biesel and her collaborators have conducted numerical and experimental studies on cell behaviors in shear flow,[22,23] and channel flows,[24,25] and their numerical results are consistent with experiments. It should be noted that these studies based on BEM are normally in creeping flow conditions. Later, the immersed boundary method (IBM) and the lattice Boltzmann method (LBM) were combined to investigate the behaviors of cells. For example, Sui and coworkers have investigated behaviors of 2D and 3D capsules in branched channels.[26,27] Xu and his collaborators have studied manipulation of cells in microfluidic devices.[12,13,28,29] Tian studied a cell in a power-law shear flow.[30] Ma et al. have developed an IB-LBM for fluid-structure interaction of cells in viscoelastic flows.[31] In addition, Ye and coworkers have made efforts on cell behaviors in bifurcated channel flows and general flows.[32,33] Other numerical methods employed in studies of cell behaviors may include the spectral method[34] and the front-tracking method,[35] etc.

The immersed boundary method was initially developed to model the blood flow in the human heart by Peskin.[36,37] In IBM, a fixed Cartesian mesh is used to describe the fluid flow, and the immersed boundary is represented by a set of Lagrangian points. A force density is spread onto the ambient fluid to account for the effect of the boundary. The lattice Boltzmann method has gained much attention due to its simple formulation and high level of scalability on parallel processing systems. This method is based on particle kinetics, and avoids discretizing the Navier-Stokes equations and handling nonlinear operators and pressure Poisson equations. It has achieved great success in the past decades and has proven to be an efficient solver for fluid dynamics.[38–42] To combine the advantages of IBM and LBM, they have been coupled in problems involving fluid–structure interactions (FSIs).[43–51] Compared with other numerical methods employed in fluid–structure interaction problems, IB-LBM has several advantages: the generation of mesh is simple, especially for complex geometries. It does not require mesh movement and regeneration when handling problems with large deformations and displacements, and the efficiency of solving FSI problems is much higher.[52] These advantages make IB-LBM an excellent method to study cell behaviors in microfluidics, where moving boundaries and complex geometries are normally involved.

In this paper, the immersed boundary-lattice Boltzmann method is utilized to investigate the capture of cells in a U-shaped sieve-based microfluidic device. The efficiency of the device on capturing cells in different conditions is examined.

The rest of the paper is arranged as follows. The problem statement and numerical description are introduced in the Problem statement and numerical description section. The validation of the present numerical method is presented in the Validation section. The parameter settings and discretization of our problem is given in the Parameter setting and discretization section. The Results and discussion section presents the results and discussion. Finally, the concluding remarks are provided in the last section.

Problem statement and numerical description

Problem statement

In this work, we numerically investigated the cell capture in a microfluidic device (as schematically shown in Figure 1(a)).

The device has seven U-shaped sieves, and each one is composed of six posts. The radius of the post is labeled with r_1. The posts are placed at a cycloid outline with a radius of r_2. It expresses the sieve size. For the arrangement of the seven sieves, one is placed at the center of the chamber, and the other six are evenly placed along with a cycloid outline with a radius of r_3. The radius of the chamber is marked with r_4, thus the diameter of the chamber is $D = 2r_4$. The width of the inlet (outlet) is h. A number of cells are randomly released at the inlet one by one. In the present study, r_1, r_2 and h are regulable parameters, and we mainly focus on the cell-trapping efficiency influenced by these three parameters.

As shown in Figure 1(b), three steps of cell capture and culture are described in detail as follows. In the loading step (b1), cells are released randomly at the inlet or initialized randomly in the chamber. Based on the proposed design, a certain amount of cells (4–8 cells) are desired to be captured evenly in each sieve. This is the first and necessary step for cell culture, and the efficiency of capturing cells involved in this step has significant effects on subsequent steps (i.e. cell distribution, growth, and proliferation). In the cell culture step (b2), cells receive nutrients from the ambient fluid to grow and gradually breed into more cells.

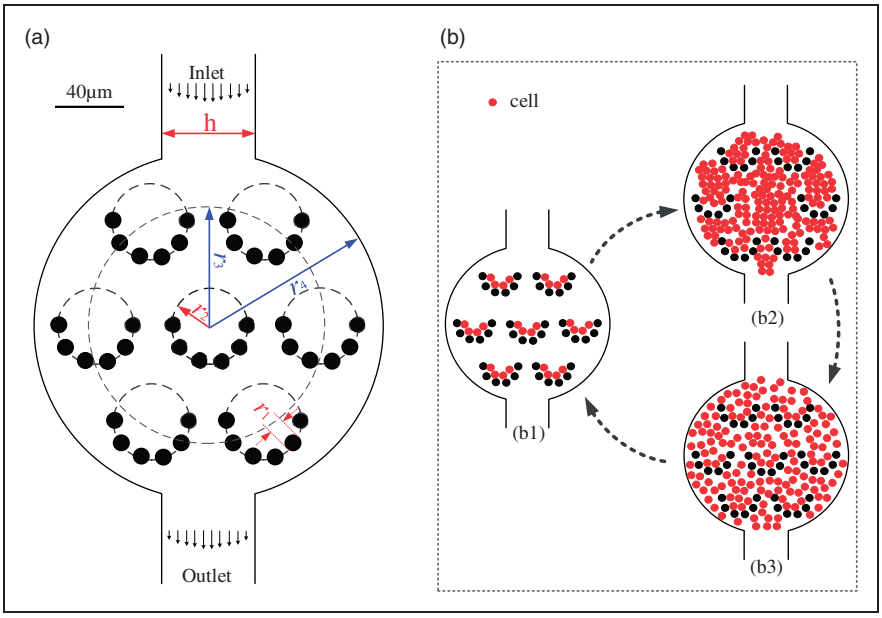

Figure 1. (a) Schematic diagram of the microfluidic device for cell capture; (b) Three steps of cell capture and culture.

Then, new cells bond together or adhere to the adjacent solid walls. In the trypsinizing step (b3), cells clinging to other surfaces can be released to the fluid by adding a finite amount of enzyme reagent into the device. Finally, enter the loading step (b1) again, in which a flow is loaded to flush most of the floating cells. Meanwhile, a few cells can be trapped by the sieves during the flushing process. The trapped cells are the seeds of the next cycle of the cell culture process. In this case, cell culture can be performed continuously by repeating steps (b1) to (b3). In this work, we mainly focus on the first step, i.e. the loading step.

The governing equations of the fluid and the cell

The dynamics of the fluid is governed by the continuity and Navier-Stokes equations

$$\nabla \cdot \boldsymbol{u} = 0 \tag{1}$$

$$\rho\left(\frac{\partial \boldsymbol{u}}{\partial t} + \boldsymbol{u} \cdot \nabla \boldsymbol{u}\right) + \nabla p = \mu \nabla^2 \boldsymbol{u} + \boldsymbol{f} \tag{2}$$

where ρ is the fluid density, $\boldsymbol{u}$ is the fluid velocity, t is time, p is the pressure, μ is the fluid viscosity, and $\boldsymbol{f}$ is the body force.

The cell is modeled as a membrane, and the equation describing the development of the forces on the membrane is[28,13]

$$\boldsymbol{F}(s,t) = \boldsymbol{F}_s(s,t) + \boldsymbol{F}_b(s,t) \tag{3}$$

where s is the arc length coordinate, $\boldsymbol{F}_s(s,t)$ and $\boldsymbol{F}_b(s,t)$ are, respectively, the elastic forces due to the stretching and bending deformation of the membrane. In this work, Hooke's law is used to evaluate the stretching force $F_s(s,t)$,[43,53] i.e.

$$\boldsymbol{F}_s(s,t) = \frac{\partial}{\partial s}\left[T(s)\frac{\partial \boldsymbol{X}(s,t)}{\partial s}\right] \tag{4}$$

where $\boldsymbol{X}(s,t)$ is the position vector of a point on the cell membrane, and $T(s)$ is the in-plain strain, and it is computed as[28]

$$T(s) = K_s\left(\left|\frac{\partial \boldsymbol{X}(s,t)}{\partial s_0}\right| - 1\right) \tag{5}$$

with K_s being the stretching coefficient of the cell membrane, and s_0 being the initial arc length. The bending component $\boldsymbol{F}_b(s,t)$ of the interfacial force is evaluated as[49]

$$\boldsymbol{F}_b(s,t) = -K_b\frac{\partial^4 \boldsymbol{X}(s,t)}{\partial s^4} \tag{6}$$

where K_b is the bending modulus of the membrane.

In this work, to handle the cell–wall and cell–cell collisions, an artificial repulsion force is introduced as[53]

$$\boldsymbol{f}(\boldsymbol{X}_i) = \begin{cases} \dfrac{K_r(\boldsymbol{X}_i - \boldsymbol{X}_j)}{\left(\min\left(|\boldsymbol{X}_i - \boldsymbol{X}_j|\right)\right)^3}, & |\boldsymbol{X}_i - \boldsymbol{X}_j| \leqslant r_c, \\ 0, & |\boldsymbol{X}_i - \boldsymbol{X}_j| > r_c \end{cases} \tag{7}$$

where K_r is a positive constant, $\boldsymbol{X}_i$ and $\boldsymbol{X}_j$ are, respectively, the position vectors of two nodes, and r_c is the critical distance for the repulsion force.

Numerical method

In this work, the fluid–structure interaction system is solved by using the immersed boundary-lattice

Boltzmann method. The discrete lattice Boltzmann equation of the single relaxation time model is in the form of[43]

$$\begin{aligned} &g_i(\boldsymbol{x}+\boldsymbol{e}_i\Delta t, t+\Delta t) - g_i(\boldsymbol{x}, t) \\ &= -\frac{1}{\tau}\left[g_i(\boldsymbol{x}, t) - g_i^{eq}(\boldsymbol{x}, t)\right] + \Delta t G_i \end{aligned} \tag{8}$$

where $g_i(\boldsymbol{x}, t)$ is the distribution function, $\boldsymbol{x}$ is the fluid parcel position, t is time, $\boldsymbol{e}_i$ is the discrete velocity along the ith direction, $g_i^{eq}(\boldsymbol{x}, t)$ is the time step, $g_i^{eq}(x, t)$ is the equilibrium distribution function, $g_i^{eq}(\boldsymbol{x}, t)$ is the non-dimensional relaxation time, and G_i is the force term exerted on the distribution function.

The D2Q9 model is used in this work, and the discrete velocities $\boldsymbol{e}_i$ are given as[54]

$$\begin{aligned} &\boldsymbol{e}_0 = (0, 0), \\ &\boldsymbol{e}_i = (\cos(\pi(i-1)/2), \sin(\pi(i-1)/2))\Delta x/\Delta t, \text{ for} \\ &\quad i = 1 \text{ to } 4, \\ &\boldsymbol{e}_i = (\cos(\pi(i-4.5)/2), \sin(\pi(i-4.5)/2))\sqrt{2}\Delta x/\Delta t, \\ &\quad \text{for } i = 5 \text{ to } 8 \end{aligned} \tag{9}$$

where Δx is the lattice spacing.

The equilibrium distribution function $g_i^{eq}(x, t)$ and the force term G_i are calculated by[49]

$$g_i^{eq} = \omega_i \rho\left[1 + \frac{\boldsymbol{e}_i \cdot \boldsymbol{u}}{c_s^2} + \frac{\boldsymbol{u}\boldsymbol{u} : (\boldsymbol{e}_i\boldsymbol{e}_i - c_s^2\boldsymbol{I})}{c_s^4}\right], \tag{10}$$

$$G_i = \left(1 - \frac{1}{2\tau}\right)\omega_i\left[\frac{\boldsymbol{e}_i - \boldsymbol{u}}{c_s^2} + \frac{(\boldsymbol{e}_i \cdot \boldsymbol{u})}{c_s^4}\boldsymbol{e}_i\right] \cdot \boldsymbol{f} \tag{11}$$

where ω_i are the weights given by $\omega_0 = 4/9$, $\omega_i = 1/9$ for $i = 1$ to 4 and $\omega_i = 1/36$ for $i = 5$ to 8, c_s is the sound speed defined by $c_s = \Delta x/\sqrt{3}\Delta t$, and $\boldsymbol{f}$ is the body force acting on the fluid.

The relaxation time τ is related to the kinematic viscosity in the Navier-Stokes equation in terms of[43,49]

$$\nu = (\tau - 0.5)c_s^2\Delta t \tag{12}$$

Once the particle density distribution is known, the fluid density, velocity, and pressure are calculated by

$$\rho = \sum_i g_i, \tag{13}$$

$$\boldsymbol{u} = \frac{\sum_i e_i g_i + 0.5\boldsymbol{f}\Delta t}{\rho}, \tag{14}$$

$$p = \rho c_s^2 \tag{15}$$

In IBM, a set of discrete marker points are used to represent the boundary geometry. The effects of the immersed boundary are taken into account by spreading the Lagrangian force onto the ambient fluid as a body force[43,49]

$$\boldsymbol{f}(\boldsymbol{x}, t) = \int_\Gamma \boldsymbol{F}(s, t) D_f(\boldsymbol{x} - \boldsymbol{X}(s, t))\mathrm{d}s \tag{16}$$

where $\boldsymbol{f}(\boldsymbol{x}, t)$ is the fluid body force density, $\boldsymbol{F}(s, t)$ is the Lagrangian force density, $D_f(\boldsymbol{x} - \boldsymbol{X}(s, t))$ is a smoothed approximation of the Dirac delta function, and it is chosen to be[43,49]

$$\begin{aligned} &D_f(\boldsymbol{x} - \boldsymbol{X}(s, t)) \\ &\quad = \frac{1}{\Delta x \Delta y}\left(\delta\left(\frac{x - X(s, t)}{\Delta x}\right)\delta\left(\frac{y - Y(s, t)}{\Delta y}\right)\right) \end{aligned} \tag{17}$$

where

$$\delta(r) = \begin{cases} \frac{\left(1 + cos\left(\frac{\pi|r|}{2}\right)\right)}{4} & |r| \leqslant 2, \\ 0 & |r| > 2 \end{cases} \tag{18}$$

The same approximation function is used to obtain the velocities of the Lagrangian nodes on the moving boundary. The mathematical form is given as

$$\boldsymbol{U}(s, t) = \int_\Omega \boldsymbol{u}(\boldsymbol{x}, t) D_f(\boldsymbol{x} - \boldsymbol{X}(s, t))\mathrm{d}\boldsymbol{x} \tag{19}$$

and the position of a node on the cell membrane is updated as

$$\frac{\partial \boldsymbol{X}(s, t)}{\partial t} = \boldsymbol{U}(s, t) \tag{20}$$

Validation

In this section, the deformation of an initially circular capsule in a simple shear flow is investigated here to validate the current method. The schematic diagram for this problem is shown in Figure 2. The initial radius of the capsule is a. The computational domain is $16a$ in length and $8a$ ($2H$) in width. The non-dimensional parameters involved in this problem are the Reynolds number $= \frac{\rho\dot{\gamma}a^2}{\mu}$, the non-dimensional shear rate $G = \frac{\mu\dot{\gamma}a}{K_s}$, and the non-dimensional bending modulus $e_b = \frac{K_b}{(a^2K_s)}$. It is noted that a different bending model is used in this problem to be consistent with Sui et al.[55] and Gou et al.,[56] but it is sufficient for the purpose of validating the present numerical method.

The grid spacing $\Delta x = \Delta y = 0.05a$ is used in the simulations. The Reynolds number used is 0.05, the non-dimensional shear rate is 0.04, and the non-dimensional bending modulus is 0, 0.025, 0.05, 0.1 and 0.2. The Taylor deformation parameter D_{xy} and

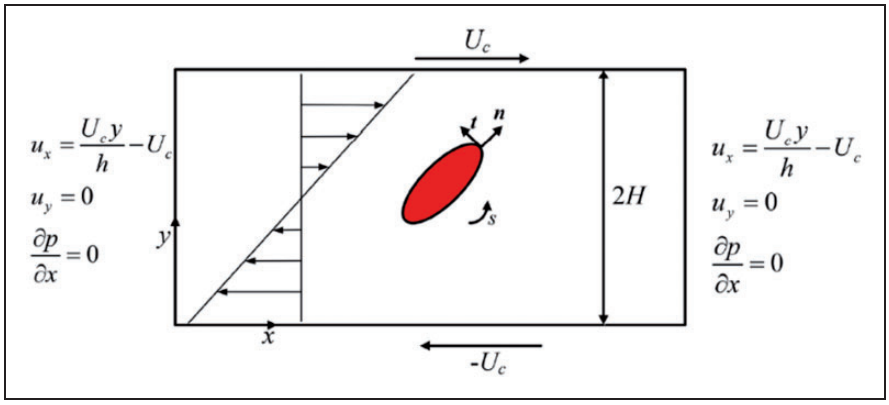

Figure 2. The schematic diagram for a capsule deformation in a simple shear flow.

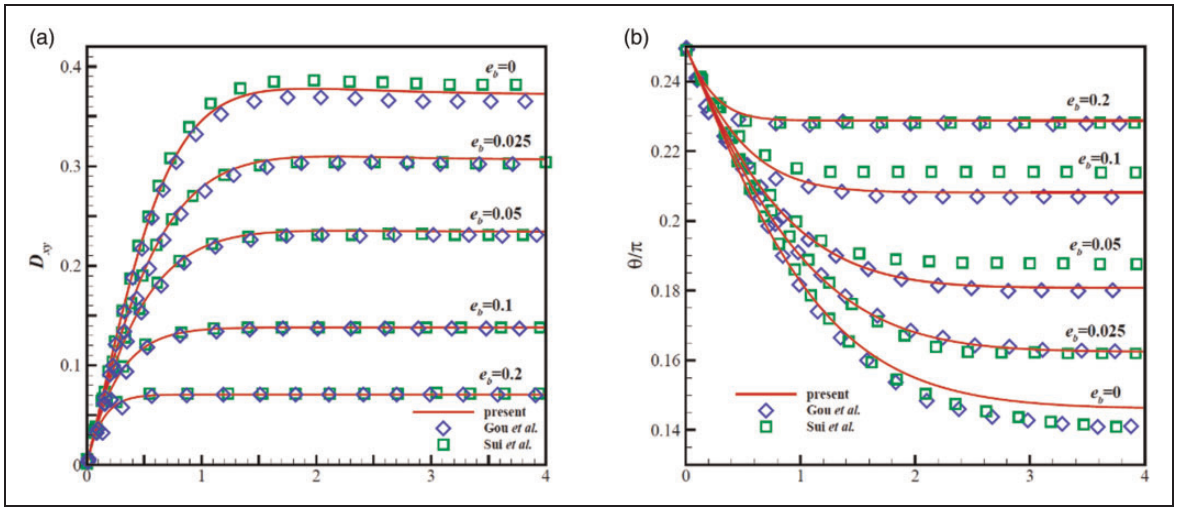

Figure 3. The temporal evolution of (a) the Taylor deformation parameter and (b) the inclination angle at G = 0.04.

the inclination angle θ are introduced to measure the deformation of the capsule. The Taylor deformation parameter is defined as $D_{xy} = (L - W)/(L + W)$, where L and W are the lengths of semi-major and semi-minor axes of the capsule, respectively. The temporal evolution of the Taylor deformation parameter D_{xy} and the inclination angle θ are compared with the results from Sui et al.[55] and Gou et al.[56] in Figure 3. It is observed that the present results show very good agreement with the previous data.

Parameter setting and discretization

In the simulations, the density of the Newtonian fluid is 1.00 g/cm^3, and the viscosity of the internal and external fluids is set as 1.2 cp. The grid spacing $\Delta x = \Delta y = 1$ in the LBM, it represents 1.2 μm in physical distance. The time step $\Delta t = 1$ in the LBM, it is 2.5×10^{-5} s in the real time scale. The other parameter settings are given as the following.

The radius of the post r_1 is set varied from 10.8 to 13.68 μm. The sieve radius r_2 is set from 21.6 to 31.2 μm. The radius of $r_3 = 76.8$ μm. The chamber radius $r_4 = 117.6$ μm. It covers 98 lattices in the LBM. The width h of the inlet (outlet) is set from 58.8 to 156.8 μm. One hundred fifty cells are randomly released at the inlet one by one. The velocity boundary is used at the inlet. The velocity is 240 μm/s (5×10^{-3} in LBM). The mass-modified-outlet boundary is applied to the outlet to conserve the mass balance to the inlet.[57] Take h as the Characteristic length, and the Reynolds number is estimated to be 0.005–0.02 in the simulations.

According to the study of Kim et al.,[8] our cell model references the BALB/3T3 cell line. Here, we choose the cell diameter as 12 μm (10 lattices in the LBM), and the spacing between two adjacent nodes on the cell is 0.96 μm. Thus 39 nodes are used to construct the cell. This size setting of the cell is suitable for our study because it can deal with larger Reynolds number cases (Re∼100).[58] In the cell membrane mechanics model, the bending rigidity K_b is set as 1.0×10^{-11}N/m (it is 0.1 in the LBM). The tension stiffness K_s is set as 2.0×10^{-11} N/m (it is 0.2 in the LBM). In the cell–wall interaction model, the adjusting coefficient K_r is set as 1.0×10^{-12} N/m (it is 0.01 in the LBM).

In order to simulate the posts (the substantial obstacles in the flow), the bounce-back condition in the

LBM framework is applied. Moreover, to handle the cell-wall collision, we attach a set of virtual boundaries on the wall surface. These virtual boundaries are made of some nodes like that of the cell membrane, which have no effect on the flow, but can prevent the cell from colliding with the wall. When a cell gets close to the virtual boundary, a repulsive force is generated through equation (7), in which the critical distance $r_c = 1.2\,\mu m$. Similarly, when two cells get close to each other, the repulsive force is also computed with equation (7), in which $r_c = 0.6\,\mu m$.

Results and discussion

Effects of the width of the inlet h

The width h of the inlet (outlet) is expected to significantly influence the efficiency of the device on capturing cells as it alters the inflow positions of cells. In this section, the effects of h on the efficiency of the device on cell capture are studied. Here $r_1 = 5.4\,\mu m$ and $r_2 = 26.4\,\mu m$. Figure 4 shows the states of cells trapped in the device after the 150 cells are totally released. It is found that the sieves in the first row (upper sieves) and two sieves in the second row can hardly capture cells when the inlet has a large width ($D/h = 1.5$). With the decrease of r_1 ($2.0 \leqslant D/h \leqslant 3.0$), cells start to be trapped in the upper sieves while the two sieves in the second row still cannot capture cells. With the further decrease of h ($D/h \geqslant 3.5$), all sieves can capture cells. This means a narrower inlet improves the efficiency of the device on trapping cells.

To further explore the effects of h on the efficiency of the device on trapping cells, the number of cells trapped in the device is used to quantify the capability of the device to capture cells. Figure 5(a) shows the number of cells trapped in the chamber as a function of D/h. It is found that the number of cells tapped in the chamber increases with D/h. In addition, it is important to achieve uniform trapping to reduce the mutual inhibition between cells and to promote their growth. In order to characterize the distribution uniformity of cells, the degree of deviation S_d is defined as

$$S_d = \sqrt{\frac{\sum_{i=1}^{N} (Cn_i - Cn_{\exp})^2}{N-1}} \tag{21}$$

where N is the total number of sieves, Cn_i is the number of cells trapped in the ith sieve, and $Cn_{\exp}$ is the expected number of cells trapped in a sieve.

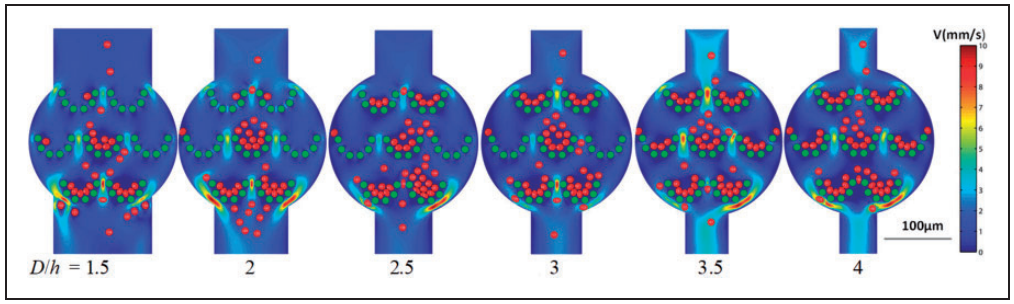

Figure 4. The instantaneous states of cells trapped in the device at different ratios of D/h.

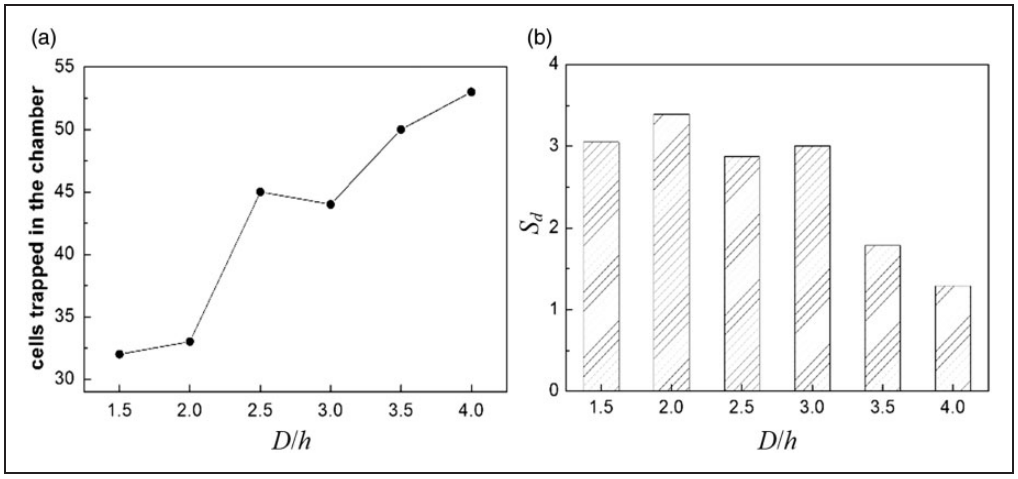

Figure 5. (a) The effects of D/h on the number of cells trapped in the chamber. (b) The effects of D/h on S_d.

According to the actual needs of the cell culture, we designed the sizes of sieves and cells. In such design, once four cells are loaded in the sieve, the flow through the sieve will be intercepted, and other cells are hard to enter the sieve with the flow. Therefore, we set $Cn_{exp}=4$ in the present study. It should be noted that a lower S_d represents a more uniform distribution. Figure 5(b) shows the degree of deviation at different D/h. It is found that S_d almost remains constant when $D/h \leqslant 3.0$. When $D/h \geqslant 3.0$, S_d experiences monotonic decrease with increasing D/h, and reaches the lowest value at $D/h = 4.0$. Therefore, to improve the capability of the device to trap cells and to achieve a uniform distribution of cells, $D/h = 4.0$ ($h = 58.8\,\mu m$) is used in the following sections.

Effects of the radius of the sieves r_2

In this section, the effects of the sieve radius r_2 on the efficiency of the device on trapping cells are investigated. Here, the width of the inlet $h = 28.8\,\mu m$ is used (as discussed in the *Effects of the width of the inlet h* section), and the radius of the posts r_1 is 5.4 μm. Here r_2 ranges from 21.6 μm to 31.2 μm with an increment of 2.4 μm. Figure 6 shows the instantaneous configurations of cells trapped in the device at different r_2. It is found that the device is not efficient in tapping cells when r_2 is small. Specifically, the upper sieves and two sieves in the second row cannot capture cells. This is caused by two reasons: (a) the sieves are not sufficiently large for efficient trapping of cells; (b) the sizes of the apertures are small (r_1 is fixed). This increases the resistance of the sieves, and cells move through regions with low resistance (gaps between sieves). With the increase of r_2 ($r_2 = 24\,\mu m$, $26.4\,\mu m$, and $28.8\,\mu m$), the device is able to capture more cells. However, with the further increase of r_2 ($r_2 = 31.2\,\mu m$), it seems that fewer cells are captured by the device. This is because the apertures between posts in the sieves become too large, and cells move through the apertures.

Figure 7(a) shows the number of cells trapped in the device as a function of the cell released at different r_2. It is found that the number of cells trapped experiences a remarkable increase at all r_2 with the increase of the number of cells released when 80 cells or less are released in the device, and it almost remains constant when more than 80 cells are released. This means the device can only capture a certain number of cells, and

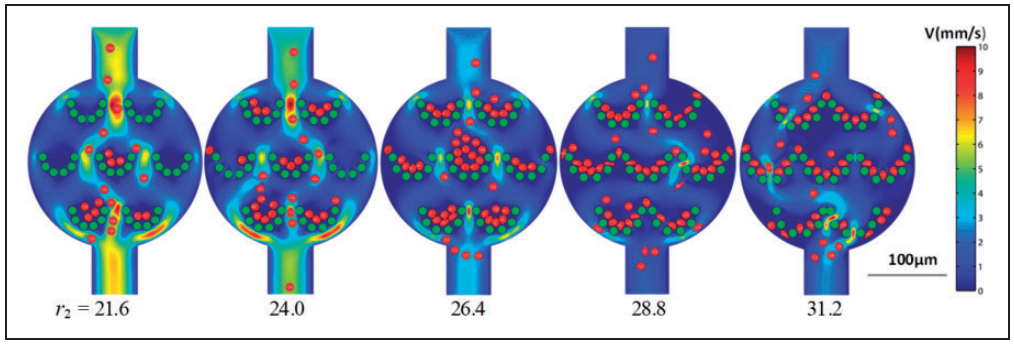

Figure 6. The instantaneous configurations of cells at $r_1 = 5.4\,\mu m$ and different r_2.

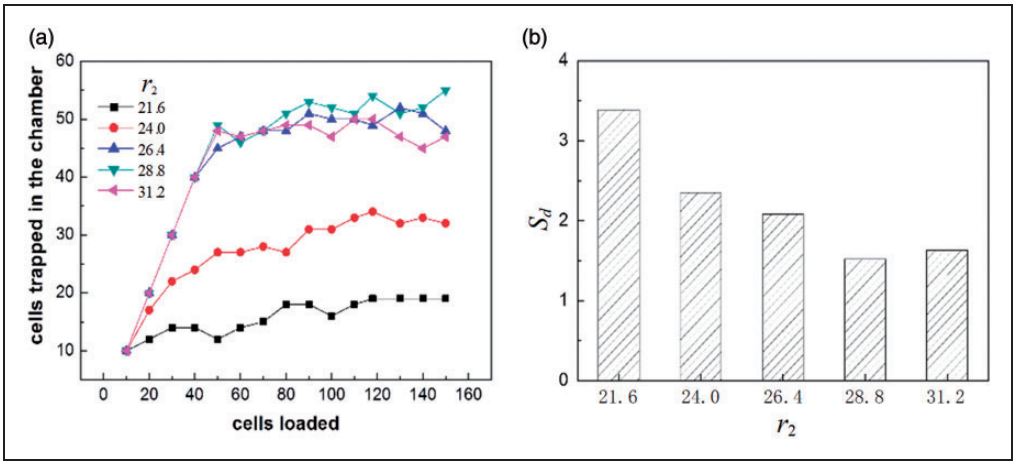

Figure 7. (a) The number of cells trapped in the chamber as a function of the cell released. (b) The degree of S_d at different radii of the sieves r_2.

if this number reaches the full capacity of the device, the device would not be able to capture more cells. This is probably due to the aperture are blocked and the resistance of sieves significantly. In addition, the device is able to capture the most cells when $r_2 = 28.8\,\mu m$. Figure 7(b) shows the dependence of the degree of deviation on r_2. It is found that the degree of deviation reaches the lowest value when $r_2 = 28.8\,\mu m$. Therefore, the device reaches the best performance on capturing cells and obtaining a uniform distribution at $r_2 = 28.8\,\mu m$.

Effects of the radius of the posts r_1

In this section, the effects of the radius of the posts r_1 on the efficiency of the device on trapping cells are investigated. The width of the inlet $h = 28.8\,\mu m$, and the radius of the sieves $r_2 = 26.4\,\mu m$ are used. The radius of the posts r_1 ranges from 5.4 μm to 6.84 μm with an increment of 0.36 μm. Figure 8 shows the instantaneous configuration of cells at different radii of the posts. It is found that the device seems to be able to capture more cells when the radius of the posts is small ($r_1 = 5.4\,\mu m$ and $5.76\,\mu m$). This is due to the large resistance of sieves caused by the small apertures. In this case, cells tend to move through the gaps between sieves (regions with low resistance).

Figure 9(a) shows the number of cells trapped in the device as a function of the number of cells released at different r_1. It is observed that the device captures more cells as r_1 increases from 5.4 μm to 5.76 μm. This is because in such size of r_1, cells can get through the apertures between the posts. However, cells are hard to cross if the size of the apertures becomes narrower at a larger r_1. With the further increase of r_1, the number of cells captured almost remains constant at different r_1. This is probably because the flow resistance of the sieves becomes the dominating parameter to determine the number of cells that the device can capture. In this case, the flow resistance of the sieves is too large that most cells tend to follow flows through the regions with low flow resistance. Figure 9(b) shows the degree of the deviation at different r_1. It is found that the degree of the deviation experiences a remarkable decrease when r_1 increases from 5.4 μm to 6.12 μm, and then increases with the further increase of r_1 from 6.12 μm to 6.84 μm. Then, in order to achieve uniform trapping of cells, the radius of the posts should be 6.12 μm.

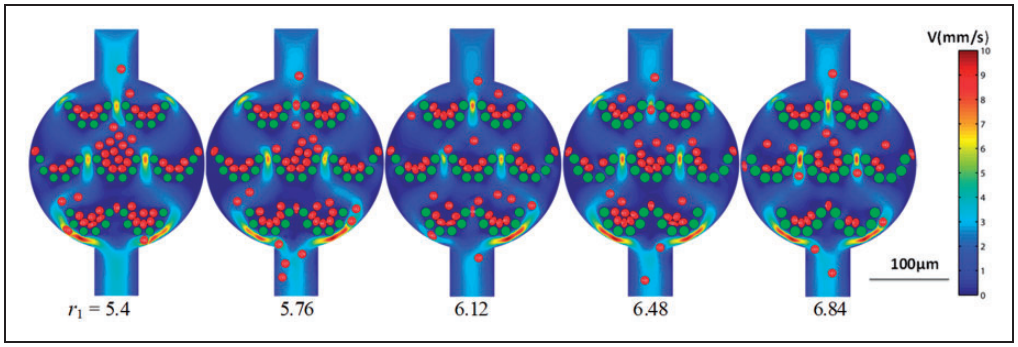

Figure 8. The configurations of cells at $r_2 = 26.4\,\mu m$ and different radius of the posts r_1.

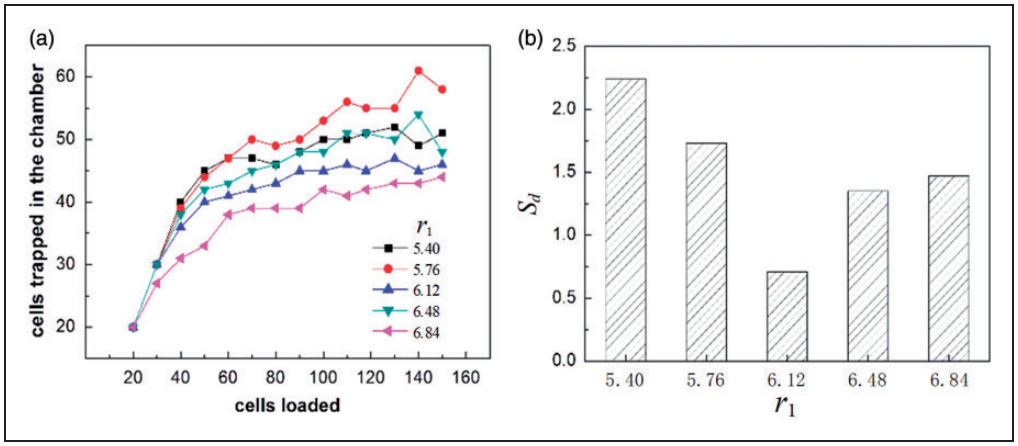

Figure 9. (a) The number of cells trapped in the chamber as a function of the number of cells released in the device at different r_1. (b) The degree of S_d at different radii of the posts r_1.

Conclusions

In conclusion, we have numerically investigated cell capture in a U-shaped sieve-based microfluidic device. The effects of the width of the inlet, the radius of the sieves, and the radius of the posts on the efficiency of the device are studied. It is found that a narrower inlet can promote the trapping of cells in the device and the uniform distribution of cells. In addition, the device is not efficient in capturing cells when the radius of the sieves (r_2) is small. And with the increase of r_2, the number of cells trapped in the device first increase and then decrease due to the resistance of the sieves and the sizes of the apertures between posts. Finally, the effects of the radius of the posts (r_1) on the efficiency of the device to capture cells are studied. It is found that the device is able to capture more cells when r increases from 5.4 μm to 5.76 μm, and the number of cells trapped in the device almost remains constant with the further increase of r_1.

Declaration of Conflicting Interests

The author(s) declared no potential conflicts of interest with respect to the research, authorship, and/or publication of this article.

Funding

The author(s) disclosed receipt of the following financial support for the research, authorship, and/or publication of this article: This work is supported by the National Natural Science Foundation of China (grant no. 81771935). J-TM would like to acknowledge the support from the Australian Research Council (ARC Discovery Early Career Researcher Award, project number DE160101098).

ORCID iD

Yuan-Qing Xu https://orcid.org/0000-0002-4482-893X

References

1. Wang X, Gou X, Chen S, et al. Cell manipulation tool with combined microwell array and optical tweezers for cell isolation and deposition. *J Micromech Microeng* 2013; 23: 075006.
2. Petersson F, Nilsson A, Holm C, et al. Separation of lipids from blood utilizing ultrasonic standing waves in microfluidic channels. *Analyst* 2004; 129: 938.
3. Guo F, Mao Z, Chen Y, et al. Three-dimensional manipulation of single cells using surface acoustic waves. *Proc Natl Acad Sci* 2016; 113: 1522.
4. Zhang C, Khoshmanesh K, Mitchell A, et al. Dielectrophoresis for manipulation of micro/nano particles in microfluidic systems. *Analytical Bioanalytical Chem* 2010; 396: 401.
5. Hunt T and Westervelt R. Dielectrophoresis tweezers for single cell manipulation. *Biomed Microdevice* 2006; 8: 227.
6. Di Carlo D, Wu LY and Lee LP. Dynamic single cell culture array. *Lab Chip* 2006; 6: 1445.
7. Skelley AM, Kirak O, Suh H, et al. Microfluidic control of cell pairing and fusion. *Nat Meth* 2009; 6: 147.
8. Kim M-C, Wang Z, Lam RH, et al. Building a better cell trap: applying Lagrangian modeling to the design of microfluidic devices for cell biology. *J Appl Phys* 2008; 103: 044701.
9. Kim M-C and Klapperich C. A new method for simulating the motion of individual ellipsoidal bacteria in microfluidic devices. *Lab Chip* 2010; 10: 2464.
10. Lu S-Y, Malekanfard A, Beladi-Behbahani S, et al. Passive dielectrophoretic focusing of particles and cells in ratchet microchannels. *Micromachines* 2020; 11: 451.
11. Sun D-K, Wang Y, Dong A-P, et al. A three-dimensional quantitative study on the hydrodynamic focusing of particles with the immersed boundary – Lattice Boltzmann method. *Int J Heat Mass Transf* 2016; 94: 306.
12. Ma JT, Xu YQ and Tang XY. A numerical simulation of cell separation by simplified asymmetric pinched flow fractionation. *Computat Math Meth Med* 2016; 2016: 8.
13. Wei Q, Xu Y-Q, Tang X-Y, et al. An IB-LBM study of continuous cell sorting in deterministic lateral displacement arrays. *Acta Mech Sinica* 2016; 32: 1023.
14. Sui Y, Chew Y, Roy P, et al. Inertia effect on the transient deformation of elastic capsules in simple shear flow. *Comput Fluids* 2009; 38: 49.
15. Ma J, Xu L, Tian F-B, et al. Dynamic characteristics of a deformable capsule in a simple shear flow. *Phys Rev E* 2019; 99: 023101.
16. Schmid-Schönbein H and Wells R. Fluid drop-like transition of erythrocytes under shear. *Science* 1969; 165: 288.
17. Abkarian M, Faivre M and Viallat A. Swinging of red blood cells under shear flow. *Phys Rev Lett* 2007; 98: 188302.
18. Dupire J, Socol M and Viallat A. Full dynamics of a red blood cell in shear flow. *Proc Natl Acad Sci* 2012; 109: 20808.
19. Ramanujan S and Pozrikidis C. Deformation of liquid capsules enclosed by elastic membranes in simple shear flow: large deformations and the effect of fluid viscosities. *J Fluid Mech* 1998; 361: 117.
20. Breyiannis G and Pozrikidis C. Simple shear flow of suspensions of elastic capsules. *Theoret Computat Fluid Dynam* 2000; 13: 327.
21. Kwak S and Pozrikidis C. Effect of membrane bending stiffness on the axisymmetric deformation of capsules in uniaxial extensional flow. *Phys Fluid* 2001; 13: 1234.
22. Lac E, Morel A and Barthes-Biesel D. Hydrodynamic interaction between two identical capsules in simple shear flow. *J Fluid Mech* 2007; 573: 149.
23. Walter J, Salsac AV, Barthès-Biesel D, et al. Coupling of finite element and boundary integral methods for a capsule in a Stokes flow. *Int J Num Meth Eng* 2010; 83: 829.
24. Hu X-Q, Salsac A-V and Barthès-Biesel D. Flow of a spherical capsule in a pore with circular or square cross-section. *J Fluid Mech* 2012; 705: 176.
25. Hu X-Q, Sévénié B, Salsac A-V, et al. Characterizing the membrane properties of capsules flowing in a square-section microfluidic channel: effects of the membrane constitutive law. *Phys Rev E* 2013; 87: 063008.
26. Wang Z, Sui Y, Salsac A, et al. Motion of a spherical capsule in branched tube flow with finite inertia. *J Fluid Mech* 2016; 806: 603.

27. Wang Z, Sui Y, Salsac A-V, et al. Path selection of a spherical capsule in a microfluidic branched channel: towards the design of an enrichment device. *J Fluid Mech* 2018; 849: 136.
28. Ma J, Xu Y, Tian F, et al. IB-LBM study on cell sorting by pinched flow fractionation. *Bio-Med Mat Eng* 2014; 24: 2547.
29. Wei Q, Xu Y-Q, Tian F-B, et al. IB-LBM simulation on blood cell sorting with a micro-fence structure. *Bio-med Mat Eng* 2014; 24: 475.
30. Tian FB. Deformation of a capsule in a power-law shear flow. *Comput Math Meth Med* 2016; 2016: 7981386.
31. Ma J, Wang Z, Young J, et al. An immersed boundary-lattice Boltzmann method for fluid-structure interaction problems involving viscoelastic fluids and complex geometries. *J Computat Phys* 2020; 415: 109487.
32. Ye H, Huang H and Lu X-Y. Numerical study on dynamic sorting of a compliant capsule with a thin shell. *Comput Fluid* 2015; 114: 110.
33. Ye H, Huang H, Sui Y, et al. Dynamics of a nonspherical capsule in general flow. *Comput Fluid* 2016; 134: 31.
34. Kessler S, Finken R and Seifert U. Swinging and tumbling of elastic capsules in shear flow. *J Fluid Mech* 2008; 605: 207.
35. Bagchi P and Kalluri RM. Dynamic rheology of a dilute suspension of elastic capsules: effect of capsule tank-treading, swinging and tumbling. *J Fluid Mech* 2011; 669: 498.
36. Peskin CS. The immersed boundary method. *Acta Numerica* 2002; 11: 479.
37. Peskin CS. Numerical analysis of blood flow in the heart. *J Computat Phys* 1977; 25: 220.
38. Chen S and Doolen G. Lattice Boltzmann method for fluid flows. *Ann Rev Fluid Mech* 1998; 30: 329.
39. Chai Z, Liang H, Du R, et al. A Lattice Boltzmann model for two-phase flow in porous media. *SIAM J Scientific Comput* 2019; 41: B746.
40. Wen B, Huang B, Qin Z, et al. Contact angle measurement in lattice Boltzmann method. *Comput Math Appl* 2018; 76: 1686.
41. Yan W, Liu Y and Fu B. LBM simulations on the influence of endothelial SGL structure on cell adhesion in the micro-vessels. *Comput Math Appl* 2019; 78: 1182.
42. Du R and Liu Z. A lattice Boltzmann model for the fractional advection–diffusion equation coupled with incompressible Navier–Stokes equation. *Appl Math Lett* 2020; 101: 106074.
43. Tian F-B, Luo H, Zhu L, et al. An efficient immersed boundary-lattice Boltzmann method for the hydrodynamic interaction of elastic filaments. *J Computat Phys* 2011; 230: 7266.
44. Tian F-B, Luo H, Zhu L, et al. Coupling modes of three filaments in side-by-side arrangement. *Phys Fluids (1994–present)* 2011; 23: 111903.
45. Tian F-B, Luo H, Zhu L, et al. Interaction between a flexible filament and a downstream rigid body. *Phys Rev E* 2010; 82: 026301.
46. Tian F-B. Role of mass on the stability of flag/flags in uniform flow. *Appl Phys Lett* 2013; 103: 034101.
47. Sun D, Wang Y, Jiang D, et al. Dynamic self-assembly of particles in an expanding channel flow. *Appl Phys Lett* 2013; 103: 071905.
48. Xu L, Tian F-B, Young J, et al. A novel geometry-adaptive Cartesian grid based immersed boundary–lattice Boltzmann method for fluid–structure interactions at moderate and high Reynolds numbers. *J Computat Phys* 2018; 375: 22.
49. Xu Y-Q, Wang M-Y, Liu Q-Y, et al. External force-induced focus pattern of a flexible filament in a viscous fluid. *Appl Math Model* 2018; 53: 369.
50. Zhu L, Yu X, Liu N, et al. A deformable plate interacting with a non-Newtonian fluid in three dimensions. *Phys Fluid* 2017; 29: 083101.
51. Liu Q-Y, Tang X-Y, Chen D-D, et al. Hydrodynamic study of sperm swimming near a wall based on the immersed boundary-lattice Boltzmann method. *Eng Appl Computat Fluid Mech* 2020; 14: 853.
52. Huang W-X and Tian F-B. Recent trends and progress in the immersed boundary method. *Proc IMechE, Part C: J Mechanical Engineering Science* 2019; 233: 7617.
53. Xu Y-Q, Tian F-B and Deng Y-L. An efficient red blood cell model in the frame of ib-lbm and its application. *Int J Biomath* 2013; 6: 1250061.
54. Sui Y, Chew YT, Roy P, et al. A hybrid method to study flow-induced deformation of three-dimensional capsules. *J Computat Phys* 2008; 227: 6351.
55. Sui Y, Chew Y, Roy P, et al. Transient deformation of elastic capsules in shear flow: effect of membrane bending stiffness. *Phys Rev E* 2007; 75: 066301.
56. Gou Z, Huang F, Ruan X, et al. Shape memory of elastic capsules under the effect of spontaneous shape. *Commun Computat Phys* 2018; 24: 234.
57. Tong CQ, He YL, Tang GH, et al. Mass modified outlet boundary for a fully developed flow in the lattice Boltzmann equation. *Int J Modern Phys C* 2007; 18: 12.
58. Sun D-K, Jiang D, Xiang N, et al. An immersed boundary-Lattice Boltzmann simulation of particle hydrodynamic focusing in a straight microchannel. *Chinese Phys Lett* 2013; 30: 074702.